ENGINEERING MECHANICS 2009
National Conference with International Participation
Svratka, Czech Republic, May 11 – 14, 2009

pp. 147–158
Paper **#201**

NUMERICAL SOLUTION OF COMPRESSIBLE FLOW PROBLEMS USING THE FINITE VOLUME FLUX-VECTOR SPLITTING SCHEMES ON UNSTRUCTURED MESHES

O. Bublík, J. Vimmr, A. Jonášová [1]

Summary: *This paper is focused on the numerical solution of the nonlinear system of the Euler equations, which describe the transonic flow of an inviscid fluid. The computation was performed using the finite volume method defined for unstructured grids. Three explicit flux-vector splitting schemes (Steger-Warming, van Leer, AUSM) are discussed. In order to improve their space accuracy, a linear reconstruction with the Barth's limiter, which was specially proposed for unstructured grids, is applied. All schemes mentioned here are compared with each other for a selected test case of transonic flow around the NACA 0012 airfoil. Further, this paper describes an algorithm of mesh adaptation for a better capturing of shock waves.*

1. Introduction

The approximation of numerical fluxes in the finite volume method plays an important role in the numerical simulation of transonic inviscid flows described by the Euler system of equations. Robustness of the resulting numerical schemes and their ability for a good capturing of the shock waves are required. The flux-vector splitting class of the numerical schemes fulfils all this requirements. These schemes have been intensively studied during the past three decades. In 80s, the first flux-vector splitting scheme was developed. Steger and Warming (Steger, 1981) presented a flux-vector splitting scheme for the system of Euler equations that was based on a generalization of the upwind scheme for the scalar hyperbolic equation. Van Leer reassumed (Leer, 1982) with the flux-vector splitting according to the normal Mach number. In 90s, Liu and Steffen (Liou, 1993) presented the AUSM (Advection Upstream Splitting Method) flux-vector splitting scheme. They showed that their scheme is very suitable for capturing of shock waves and they compared it with the Roe's scheme.
This paper deals with the numerical solution of the nonlinear system of the Euler equations, describing the transonic inviscid flow, using the finite volume method defined for unstructured meshes. The contents of this paper follows the previous work found in (Hajžman, 2007). A

[1] Ing. Ondřej Bublík, Ing. Jan Vimmr Ph.D., Ing. Alena Jonášová, Department of Mechanics, Faculty of Applied Sciences, University of West Bohemia, Univerzitní 22, 30614 Plzeň 9, tel. +420 377 63 23 98, e-mail obublik@kme.zcu.cz

well-known test case of transonic flow around the NACA 0012 airfoil was selected and numerically solved applying the Steger-Warming, van Leer and AUSM schemes, whose first order space accuracy was improved to the second order by the linear reconstruction with the Barth's limiter. The objective of this paper is to perform a comparison of numerical results obtained with the developed software. The main contribution of our work lies in the application of mesh adaptation algorithm in order to be able to good capture shock waves.

2. Governing equations

The mathematical model of a compressible inviscid fluid flow is described by the nonlinear conservative system of the Euler equations. In the two-dimensional Cartesian coordinate system, we can write the system of equations in the form

$$\frac{\partial \mathbf{w}}{\partial t} + \frac{\partial \mathbf{f}(\mathbf{w})}{\partial x} + \frac{\partial \mathbf{g}(\mathbf{w})}{\partial y} = 0, \tag{1}$$

$$\mathbf{w} = \begin{pmatrix} \rho \\ \rho u \\ \rho v \\ \rho E \end{pmatrix}, \qquad \mathbf{f}(\mathbf{w}) = \begin{pmatrix} \rho u \\ \rho u^2 + p \\ \rho uv \\ \rho uH \end{pmatrix}, \qquad \mathbf{g}(\mathbf{w}) = \begin{pmatrix} \rho v \\ \rho uv \\ \rho v^2 + p \\ \rho vH \end{pmatrix}, \tag{2}$$

where $\mathbf{w}$ is the vector of conservative variables, $\mathbf{f}(\mathbf{w})$, $\mathbf{g}(\mathbf{w})$ are the inviscid fluxes in the x and y directions respectively. The relation between the enthalpy and the total energy can be defined as $H = E + p/\rho$. The system of equations is closed by the constitutive relation defined for an ideal gas

$$p = (\kappa - 1)\left[\rho E - \frac{1}{2}\rho\left(u^2 + v^2\right)\right], \tag{3}$$

where $\kappa = 1.4$ is the Poisson's constant.

3. Numerical method

In this section, the discretization of the Euler equations using the cell centered finite volume method on unstructured mesh is described. The numerical schemes based on flux-vector splitting techniques is used. Since the standard flux-vector splitting schemes are only first order of accurate in space, we establish a linear reconstruction with Barth's limiter in order to increase the spatial accuracy to second order. For good capturing of shock wave, we present an adaptive mesh refinement. In order to speed up the numerical solution, we use local time stepping.

3.1. Finite volume method

The computational domain $\Omega \in R^2$ is divided into a finite number of non-overlapping control volumes Ω_k, which satisfy $\bigcup_{k=1}^{N} \Omega_k = \Omega$. In this paper, control volumes with triangular shape only are considered. Integrating every equation of the system (1) over the control volume Ω_k and using the Gauss-Ostrogradski Theorem to the approximation of fluxes we obtain the basic semidiscrete scheme of finite volume method

$$\frac{d\mathbf{w}_k}{dt} = -\frac{1}{|\Omega_k|}\sum_{j=1}^{3}\left(\mathbf{f}_j n_{xj} + \mathbf{g}_j n_{yj}\right)|\Delta\Gamma_j| = \mathbf{R}_k(\mathbf{W}), \tag{4}$$

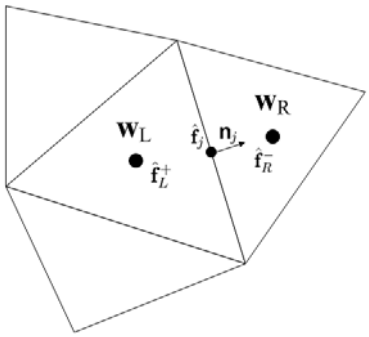

Figure 1: The splitting of the flux.

where $\mathbf{w}_k = \frac{1}{|\Omega_k|}\int_{\Omega_k} \mathbf{w}dxdy$ is an average of $\mathbf{w}$ on the control volume Ω_k, $\mathbf{n}_j = (n_{xj}, n_{yj})^T$ is the outward normal vector, $|\Delta\Gamma_j|$ is the edge length, $|\Omega_k|$ is the volume of triangular cell Ω_k , $\mathbf{f}_j$, $\mathbf{g}_j$ are numerical fluxes. The index j corresponding with j-th edge of the triangular control volume. With $\mathbf{W}$ we denote the vector $(\mathbf{w}_1, \mathbf{w}_1, \ldots, \mathbf{w}_n)^T$.

3.2. Approximations of numerical fluxes

In the two dimensional case, we establish a numerical flux $\hat{\mathbf{f}}$ as

$$\hat{\mathbf{f}} = \mathbf{f}n_x + \mathbf{g}n_y = V_n \begin{pmatrix} \rho \\ \rho u \\ \rho v \\ \rho H \end{pmatrix} + p \begin{pmatrix} 0 \\ n_x \\ n_y \\ 0 \end{pmatrix}, \tag{5}$$

where $V_n = un_x + vn_y$ is the convective velocity normal to the appropriate cell face.
The flux-splitting schemes for the systems of hyperbolic equations are generalization of the upwind scheme for the scalar hyperbolic equations (Hirsch, 1990). The basic idea is to split the flux $\hat{\mathbf{f}}$ into two parts $\hat{\mathbf{f}}^+$ and $\hat{\mathbf{f}}^-$. Then we define the flux through j-th edge of the control volume Ω_k as

$$\hat{\mathbf{f}}_j = \hat{\mathbf{f}}_L^+ + \hat{\mathbf{f}}_R^-, \tag{6}$$

where the indexes L, R denote the values of $\hat{\mathbf{f}}^{\pm}$ in the left and right control volumes, having a common edge j. The left L and right R signification of adjacent control volumes is shown in (Fig.1).

Before we start to describe the flux-splitting schemes mentioned above, let us introduce some basic definitions and useful assertion. Let $\mathbf{K} = \frac{\partial \hat{\mathbf{f}}(\mathbf{W})}{\partial \mathbf{W}}$ be the Jacobi matrix of the flux $\hat{\mathbf{f}}$. Further we define $\lambda^+ = \max(\lambda, 0)$ and $\lambda^- = \min(\lambda, 0)$. It is obvious that $\lambda^+ + \lambda^- = \lambda$ and $\lambda^+ - \lambda^- = |\lambda|$. If $\mathbf{\Lambda}$ is a $m \times n$ matrix, then $\mathbf{\Lambda}^+$ denotes $\mathbf{\Lambda}^+_{i,j} = \max(\mathbf{\Lambda}_{i,j}, 0),\ i = 1, 2, \ldots, m,\ \ j = 1, 2, \ldots, n$. Similarly for $\mathbf{\Lambda}^-$. Since $\hat{\mathbf{f}}$ is a homogenous form of order one, the relation $\hat{\mathbf{f}}(\mathbf{w}) = \mathbf{K}(\mathbf{w})\mathbf{w}$ is valid.

Steger-Warming scheme

Steger and Warming (Steger, 1981) directly used the idea of upwind scheme for the scalar hyperbolic equation. The matrix $\mathbf{K}$ is transformed by matrix $\mathbf{R}$ as

$$\mathbf{\Lambda} = \mathbf{R}^{-1}\mathbf{K}\mathbf{R}, \tag{7}$$

where the matrix $\mathbf{\Lambda}$ is diagonal with eigenvalues of $\mathbf{K}$ at the diagonal. Columns of matrix $\mathbf{R}$ consists of eigenvectors of $\mathbf{K}$. Now we can resolve matrix $\mathbf{\Lambda}$ as

$$\mathbf{\Lambda} = \mathbf{\Lambda}^{+} + \mathbf{\Lambda}^{-}. \tag{8}$$

A backward transformation of (8) gives

$$\mathbf{K} = \mathbf{R}(\mathbf{\Lambda}^{+} + \mathbf{\Lambda}^{-})\mathbf{R}^{-1} = \mathbf{R}\mathbf{\Lambda}^{+}\mathbf{R}^{-1} + \mathbf{R}\mathbf{\Lambda}^{-}\mathbf{R}^{-1} = \mathbf{K}^{+} + \mathbf{K}^{-}. \tag{9}$$

Considering the homogenity of flux $\hat{\mathbf{f}}$, we can write

$$\hat{\mathbf{f}} = \mathbf{K}\mathbf{w} = \mathbf{K}^{+}\mathbf{w} + \mathbf{K}^{-}\mathbf{w} = \hat{\mathbf{f}}^{+} + \hat{\mathbf{f}}^{-}. \tag{10}$$

This procedure leads from the system of the Euler equations to the following relation

$$\hat{\mathbf{f}}^{\pm}_{SW} = \frac{\rho}{2\kappa}\begin{pmatrix} \alpha \\ \alpha u + a(\lambda_2^{\pm} - \lambda_3^{\pm})n_x \\ \alpha v + a(\lambda_2^{\pm} - \lambda_3^{\pm})n_y \\ \alpha\frac{u^2+v^2}{2} + aV_n(\lambda_2^{\pm} - \lambda_3^{\pm}) + a^2\frac{(\lambda_2^{\pm}+\lambda_3^{\pm})}{\kappa-1} \end{pmatrix}, \tag{11}$$

where $\lambda_1 = V_n$, $\lambda_2 = V_n + a$, $\lambda_3 = V_n - a$ are eigenvalues of the matrix $\mathbf{K}$, $\alpha = 2(\kappa-1)\lambda_1^{\pm} + \lambda_2^{\pm} + \lambda_3^{\pm}$, $V_n = un_x + vn_y$ is the normal velocity projection and $a = \sqrt{\kappa p/\rho}$ is the speed of sound.

Van-Leer scheme

In the Van-Leer scheme (Leer, 1982), we split the flux according to the normal projection of the Mach number $M_n = \frac{V_n}{a} = \frac{un_x+vn_y}{a}$. We define the split mass flux component as

$$f^{\pm} = \pm\frac{\rho a(M_n \pm 1)^2}{4}. \tag{12}$$

Then we can write for the split fluxes

$$\hat{\mathbf{f}}^{\pm}_{VL} = f^{\pm}\begin{pmatrix} 1 \\ u + \frac{(-V_n \pm 2a)n_x}{\kappa} \\ v + \frac{(-V_n \pm 2a)n_y}{\kappa} \\ \frac{q^2-V_n}{2} + \frac{[(\kappa-1)V_n \pm 2a]^2}{2(\kappa^2-1)} \end{pmatrix}, \tag{13}$$

where $q^2 = u^2 + v^2$.

AUSM scheme

The AUSM scheme is similar to the Van-Leer scheme. The basic difference between both schemes comes from observations that the flux in (5) consists of two physically distinct parts: the convective part and the pressure part. The AUSM scheme (Liou, 1993) and (Liou, 2000) splits both parts in different manner. Let we again introduce the normal Mach number as in the case of van Leer splitting

$$M_n = \frac{V_n}{a}, \tag{14}$$

we can rewrite the expression (5) as

$$\hat{\mathbf{f}} = M_n \begin{pmatrix} \rho a \\ \rho a u \\ \rho a v \\ \rho a H \end{pmatrix} + p \begin{pmatrix} 0 \\ n_x \\ n_y \\ 0 \end{pmatrix}. \tag{15}$$

Further, we define the interface normal Mach number

$$M_{L/R} = \mathcal{M}^+(M_{nL}) + \mathcal{M}^-(M_{nR}), \tag{16}$$

where $\mathcal{M}^+$, $\mathcal{M}^-$ are the Mach number splitting functions defined as

$$\mathcal{M}^{\pm} = \begin{cases} \frac{1}{2}(M \pm |M|), & \text{if } |M| > 0 \\ \pm\frac{1}{4}(M \pm 1)^2 \pm \frac{1}{8}(M^2-1)^2, & \text{otherwise} \end{cases}. \tag{17}$$

For the pressure term we define the interface pressure as

$$p_{L/R} = \mathcal{P}^+(M_{nL}) \cdot p_L + \mathcal{P}^-(M_{nR}) \cdot p_R, \tag{18}$$

where

$$\mathcal{P}^{\pm} = \begin{cases} \frac{1}{2}(M \pm |M|)/M, & \text{if } |M| > 0 \\ \pm\frac{1}{4}(M \pm 1)^2(2 \mp M), & \text{otherwise} \end{cases}. \tag{19}$$

Now we can write for the split part of the flux

$$\hat{\mathbf{f}}^+_{AUSM} = M^+_{L/R} \begin{pmatrix} \rho a \\ \rho a u \\ \rho a v \\ \rho a H \end{pmatrix}_L + \frac{p_{L/R}}{2} \begin{pmatrix} 0 \\ n_x \\ n_y \\ 0 \end{pmatrix}, \quad \hat{\mathbf{f}}^-_{AUSM} = M^-_{L/R} \begin{pmatrix} \rho a \\ \rho a u \\ \rho a v \\ \rho a H \end{pmatrix}_R + \frac{p_{L/R}}{2} \begin{pmatrix} 0 \\ n_x \\ n_y \\ 0 \end{pmatrix} \tag{20}$$

3.3. Improvement of spatial accuracy

All flux-splitting schemes mentioned above are only first order accurate in space. In order to increase the accuracy from the first order to the second order, the linear reconstruction is used. To keep the monotonicity and thus to prevent spurious oscillations, the reconstructed values are not allowed to exceed the maximum and minimum of neighbouring centroid values. This is achieved by addition of the Barth's limiter (Barth, 1989)

$$\mathbf{w}_{kj} = \mathbf{w}_k + \sigma_{Barth} \nabla \mathbf{w}_k \mathbf{r}_j, \tag{21}$$

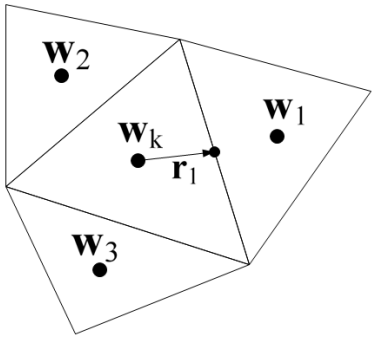

Figure 2: Significations of neighbouring control volumes at linear reconstruction by the Barth's limiter.

where $\mathbf{w}_{kj}$ is the reconstructed value of $\mathbf{w}_k$ on the j-th edge, $\mathbf{r}_j$ is the vector connecting the center of control volume with the center of j-th edge, σ_{Barth} is the Barth's limiter defined as

$$\sigma_{Barth} = \min_j \begin{cases} \min\left(1, \frac{\mathbf{w}_{\max}-\mathbf{w}_k}{\nabla \mathbf{w}_k \mathbf{r}_j}\right), & \text{if } \nabla \mathbf{w}_k \mathbf{r}_j > 0, \\ \min\left(1, \frac{\mathbf{w}_{\min}-\mathbf{w}_k}{\nabla \mathbf{w}_k \mathbf{r}_j}\right), & \text{if } \nabla \mathbf{w}_k \mathbf{r}_j < 0, \\ 1, & \text{if } \nabla \mathbf{w}_k \mathbf{r}_j = 0, \end{cases} \tag{22}$$

where $\mathbf{w}_{\max} = \max(\mathbf{w}_k, \mathbf{w}_1, \mathbf{w}_2, \mathbf{w}_3)$, $\mathbf{w}_{\min} = \min(\mathbf{w}_k, \mathbf{w}_1, \mathbf{w}_2, \mathbf{w}_3)$ according to (Fig.2).

3.4. Time integration

For the time integration of (4), the explicit two stage Runge-Kutta method of the second order of accuracy is used.

$$\begin{aligned} \mathbf{K}_1 &= \mathbf{R}(\mathbf{W}^n), \\ \mathbf{K}_2 &= \mathbf{R}(\mathbf{W}^n + \Delta t \mathbf{K}_1), \\ \mathbf{W}^{n+1} &= \mathbf{W}^n + \frac{1}{2}\Delta t(\mathbf{K}_1 + \mathbf{K}_2). \end{aligned} \tag{23}$$

3.5. Adaptive mesh refinement

The mesh adaptation can be described in this four basic steps, see (Fig.3):

1. We have to mark those control volumes (elements) that should be divided. For the marking, we use a monitor function chosen according to the purpose of the mesh adaptation. In this paper, we apply a monitor function designed specially for the indication of shock waves. These elements are displayed with darker colors in (Fig.3a).

2. Every edge, which is a part of one of these chosen elements, is marked, see (Fig.3b).

3. Every element of the computational mesh has to be composed of either three, one or no marked edges. If some element does not satisfy this condition, an additional edge of this element is also marked. An example of this situation is showed in (Fig.3b,c).

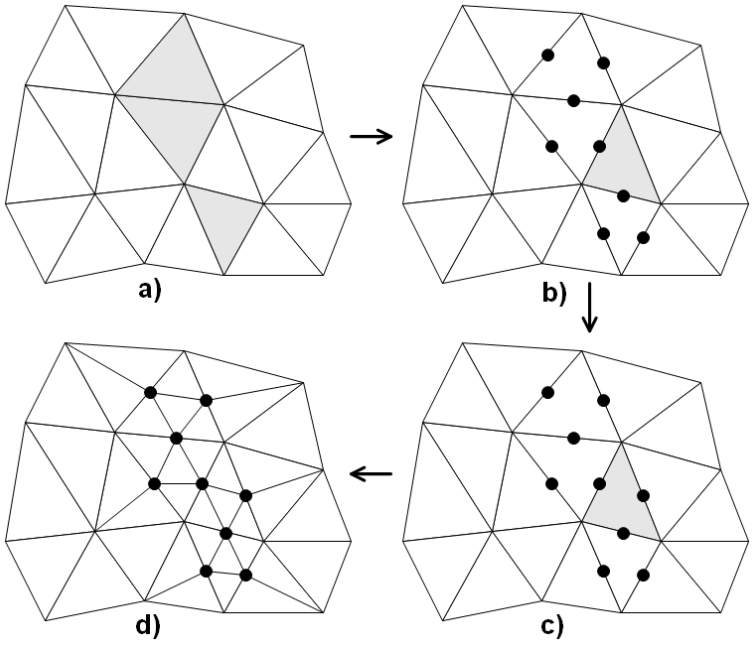

Figure 3: The mesh adaptation procedure.

4. Now the marked elements can be divided accordingly to these rules. For an element with three marked edges, the mesh adaptation is performed in the form of four new elements that originate by connecting the edge centers with each other. In the case of an element with one marked edge, the connection of marked edge center with the vertex on the opposite side of the element leads to two new elements, see (Fig.3d).

Within this paper, we use the monitor function (Feistauer, 2003)

$$g_k^{shock} = \max_j \frac{((\rho_j - \rho_k)\mathbf{v}_k\mathbf{n}_j)^+}{h_{kj}}, \tag{24}$$

where ρ_j is the density in the j-th neighbour's control volume, $\mathbf{v} = (u, v)^T$ is the velocity vector, $\mathbf{n}_j$ is the outward normal vector of the j-th edge and h_{kj} is the distance between centers of gravity of k and j neighboring control volumes. The function g^{shock} has the higher value in places, where the shock waves are present. The control volume will become marked if

$$g_k^{shock} > \varepsilon, \tag{25}$$

where $\varepsilon > 0$ is a given toleration.

3.6. Local time stepping

The CFL condition of stability in the control volume has the form

$$\Delta t_k < \frac{CFL}{\frac{|\lambda_{Ak}|+|\lambda_{Bk}|}{\Delta l_k}}, \tag{26}$$

where λ_{Ak}, λ_{Bk} are the maximal eigenvalues of matrices $\frac{\partial \mathbf{f}(\mathbf{w}_k)}{\partial \mathbf{w}}$ and $\frac{\partial \mathbf{g}(\mathbf{w}_k)}{\partial \mathbf{w}}$, Δl_k is the diameter of control volume Ω_k.

For the time depend computation, we must state $\Delta t = \min_k(\Delta t_k)$ for each control volume. We can see that the presence of small control volumes affects very negatively the size of the resultant time step. If we are interested only in the steady-state solution, we can set the local time step Δt_k for each control volume Ω_k.

4. Numerical results

Firstly, we compare our numerical results obtained using the AUSM, Steger-Warming and van Leer flux-vector splitting schemes with the linear reconstruction by the Barth's limiter on the well known test case of transonic flow around the NACA 0012 airfoil. For the application of free stream boundary conditions, we choose the computational domain in the form of a square region, whose proportion is twenty times larger than the airfoil chord. The NACA 0012 airfoil is situated in the region center. At the inlet we prescribe the Mach number $M_\infty = 0.85$ and the angel of attack $\alpha = 1^\circ$ following this the pressure at the outlet is computed. We discretized the computational domain with triangular control volumes, see (Fig.4). This generated mesh was used for all computations with the numerical schemes mentioned above. The Mach number distribution in the computational domain obtained by the application of the AUSM scheme can be found in (Fig.5). The comparison of the Mach number along upper and lower surfaces is shown in (Fig.6). We can see that AUSM scheme and the van Leer scheme lead to slightly higher maximal values of the Mach number than the Steger-Warming scheme. On the other hand, the Steger-Warming scheme was able to better catch the Zierep singularity at the lower and upper surfaces of the airfoil. Further, we can observe some oscillations of the van Leer scheme in the front part of the airfoil.

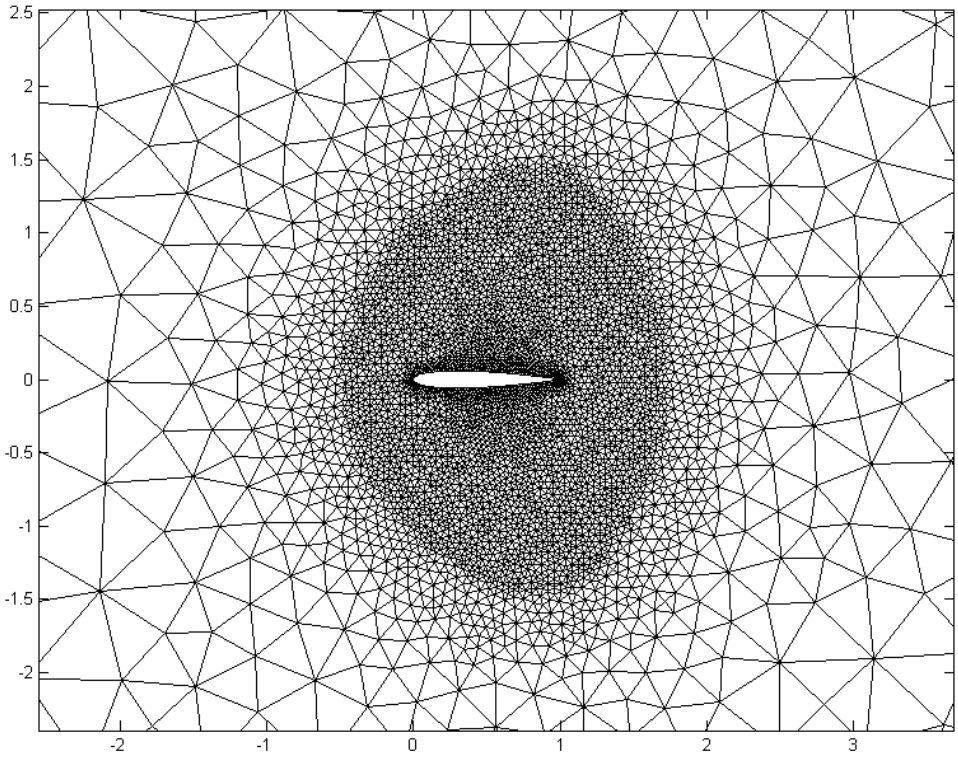

Figure 4: Detail of the unstructured mesh around the NACA 0012 airfoil.

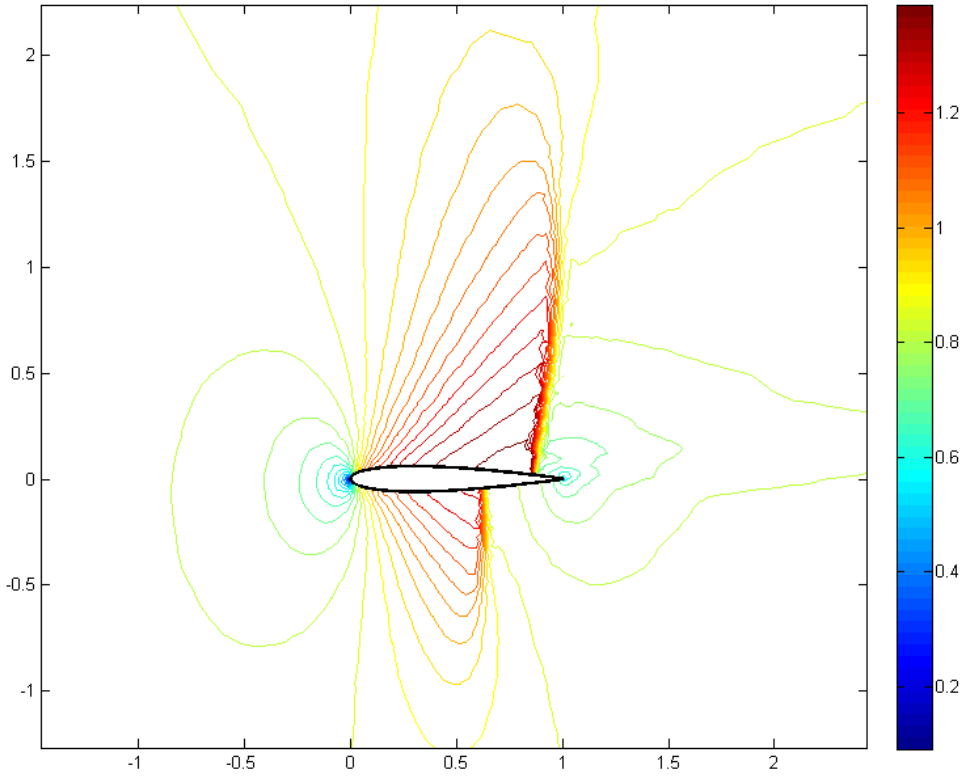

Figure 5: Distribution of the Mach number in the computational domain computed by AUSM scheme with the linear reconstruction by the Barth's limiter ($M_\infty = 0.85$, $\alpha = 1°$).

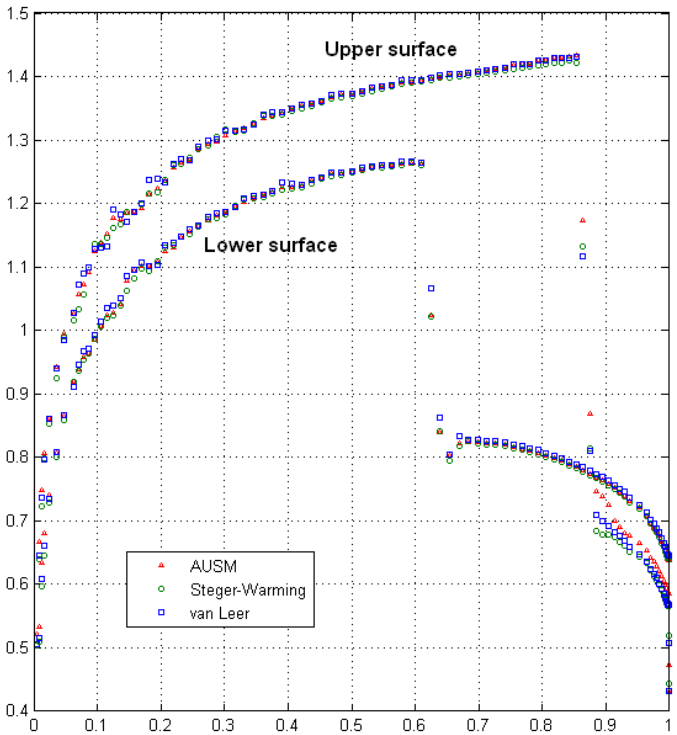

Figure 6: Comparison of the Mach number distribution on the upper and lower surface of the NACA 0012 airfoil ($M_\infty = 0.85$, $\alpha = 1°$).

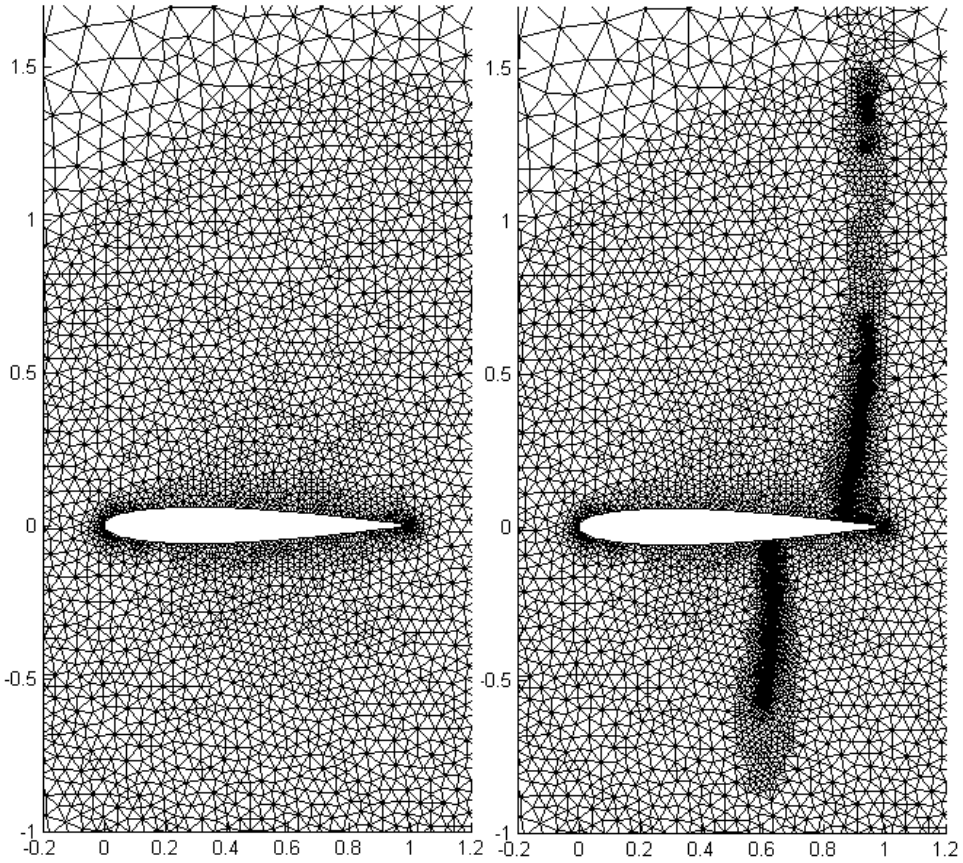

Figure 7: Comparison of details of adapted and unadapted meshes.

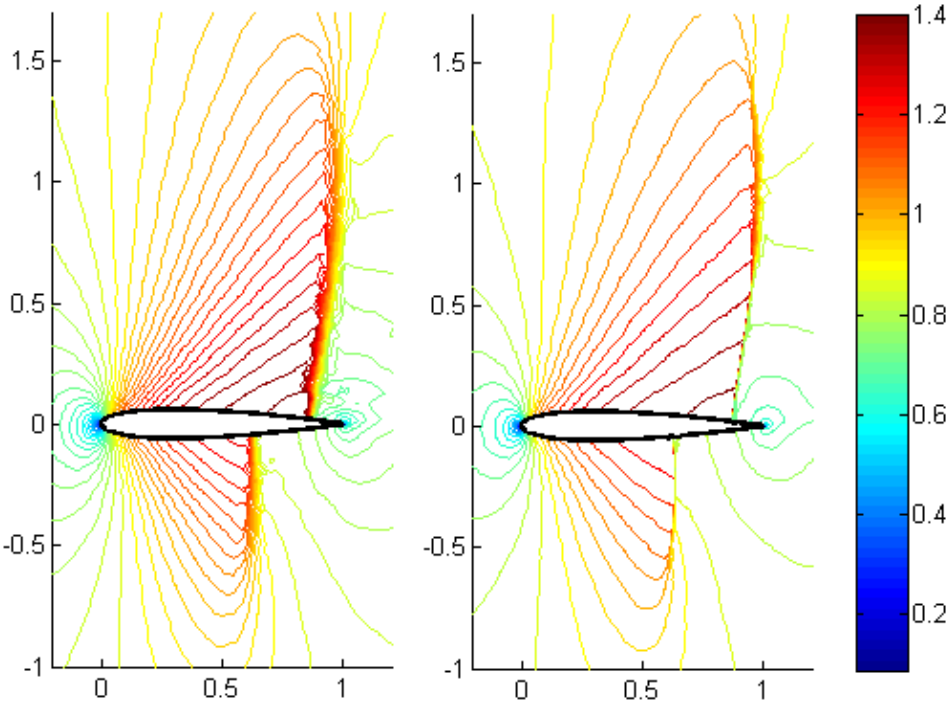

Figure 8: Comparison of distribution of the Mach number for adapted and unadapted meshes using the AUSM scheme with the linear reconstruction by the Barth's limiter ($M_\infty = 0.85$, $\alpha = 1°$).

Now we will deal with comparison of numerical solutions on the adapted and the unadapted mesh obtained with the AUSM scheme with the linear reconstruction by the Barth's limiter. We consider the same geometry and the same boundary conditions that were mentioned in the case above. (Fig.7) shows the detail of the mesh before and after the adaptation process. We can see that the local refinement is in the place where the shock waves are present. In (Fig.8) is comparison of the Mach number isolines in the computation domain computed using the AUSM scheme with the linear reconstruction by the Barth's limiter for both adapted and unadapted mesh. (Fig.9) shows distribution of the Mach number along the upper and the lower surfaces of the airfoil for adapted and unadapted mesh. We can see that the adaptation lead to better catch the Zierep singularity on the upper surface and to sharper shock waves.

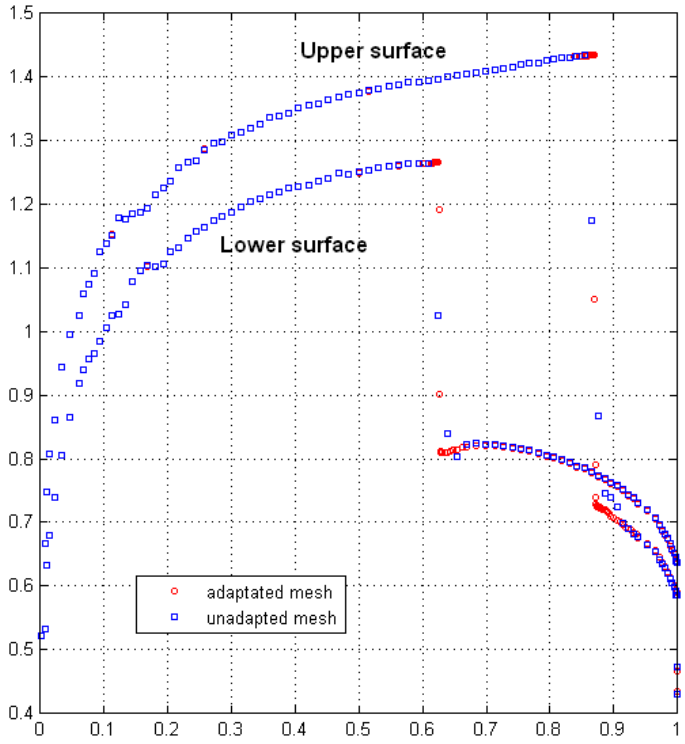

Figure 9: Comparison of the Mach number distribution on the upper and lower surfaces of the NACA 0012 airfoil for adapted and unadapted meshes.

5. Conclusion

In regard to the numerical solution of transonic inviscid flow around the NACA 0012 airfoil, a qualitative comparison of three flux-vector splitting schemes with linear reconstruction by the Barth's limiter was performed on triangular mesh. The obtained numerical results showed that all presented schemes are able to capture shock waves and that they are suitable for transonic problems on unstructured meshes. The AUSM and the van Leer schemes achieved higher values of the maximal Mach number. On the other hand, the Steger-Warming scheme was able to better capture the Zierep singularity. Further, a comparison of numerical results obtained with the AUSM scheme was performed for an adapted and unadapted mesh. It is obvious that the application of adapted mesh led to sharper shock waves and to a better capture of the Zierep singularity.

Within this study, we developed a software based on flux-vector splitting schemes. Due to the user-friendly interface and the simple code written in MATLAB, the software can be used not only for scientific purposes but also for education.

6. Acknowledgment

The support of project FRVŠ 958/2009/G1 is gratefully acknowledged.

7. References

Barth, T.J., Jesperson, D.C 1989: *The design and application of upwind schemes on unstructured meshes.* AIAA Paper, 89(0366).

Feistauer, F., Felcman J., Straškraba I. 2003: *Mathematical and Computational Methods for Compressible Flow.* Oxford university press 2003.

Hajžman, M., Bublík, O., Vimmr, J.: *On the modelling of compressible inviscid flow problems using AUSM schemes.* Applied and Computational Mechanics, Vol. 1, No. 2, pp. 469-478.

Hirsch, C. 1990: *Numerical computation of internal and external flows.* Vol. 1, 2, John Wiley & Sons, Chichester.

van Leer, B. 1982: *Flux-vector splitting for the Euler equations.* In Lecture Notes in Physics, Vol. 170 (Springer-Verlag, Berlin), p. 507.

Liou, M.-S., Steffen, C.J. 1993: *A new flux splitting scheme.* J. Comput. Phys. **107**, 23.

Liou, M.-S. 2000: *Mass Flux Schemes and Connection to Shock Instability.* Journal of Computational Physic **160**, 623-648.

Steger, J., Warming, R. 1981: *Flux vector splitting of the inviscid gas-dynamic equations with application to finite difference methods* J. Comput. Phys. 40 (1981), 263-293.